ISSN 1069-3513, Izvestiya, Physics of the Solid Earth, 2007, Vol. 43, No. 11, pp. 905–921. © Pleiades Publishing, Ltd., 2007.
Original Russian Text © V.I. Melnikova, N.A. Radziminovich, N.A. Gileva, A.V. Chipizubov, A.A. Dobrynina, 2007, published in Fizika Zemli, 2007, No. 11, pp. 3–20.

Activation of Rifting Processes in the Northern Cis-Baikal Region: A Case Study of the Kichera Earthquake Sequence of 1999

V. I. Melnikova[a], N. A. Radziminovich[a], N. A. Gileva[b], A. V. Chipizubov[a], and A. A. Dobrynina[a]

[a] *Institute of the Earth's Crust (IEC), Siberian Division (SD), Russian Academy of Sciences (RAS),ul. Lermontova 128, Irkutsk, 664033 Russia*

[b] *Baikal Branch, Geological Service (GS), SD, RAS, Irkutsk, Russia*

Received July 5, 2006

Abstract—The paper addresses the spatiotemporal development of the Kichera sequence of earthquakes of 1999 (more than 6000 events over the year) within the Kichera depression, terminating on land in the Northern Baikal basin; the series was the most intense of all earthquake sequences recorded in the Northern Cis-Baikal region (NCBR) since 1960. The spatial coordinates of earthquakes showed that the source rupture, originating in the area of the Kichera-Upper Angara interbasin mountainous isthmus, propagated in the SW direction toward Lake Baikal. Stresses in the sources of the two strongest shocks (Mw = 6.0 and 5.6) of the sequence were released along fault planes striking NE (normal type) and E–W (normal–strike-slip type). Focal mechanisms of aftershocks revealed the presence of differently oriented faults motions on which were controlled by a large rifting fault striking NE. The Kichera earthquakes are shown to have occurred under seismotectonic conditions dominated by NW–SE extension and to have been accompanied by active normal faulting promoting longitudinal growth of the Upper Angara depression and deepening of the Kichera depression. The seismotectonic strain rates calculated for the NCBR before and after 1999 were of the order of $(0.1–1.0) \times 10^{-10}$ yr^{-1}, whereas their values were two to three orders larger during 1999. Thus, the Kichera earthquakes confirmed the high seismic potential of the NCBR and showed that this rift segment developed through growth of depressions and destruction of interbasin mountainous isthmuses.

PACS numbers: 91.30.Dk

DOI: 10.1134/S1069351307110018

INTRODUCTION

The Northern Cis-Baikal region (55.00°–56.50°N, 109.00°–112.00°E), below referred to as the NCBR, belongs to the central (Baikal–Muya) segment of the Baikal rift zone (BRZ). It has a peculiar history: a younger age as compared with the Southern and Central basins of Lake Baikal, specific structural features of the basement developed on the platform flank of the lithospheric suture, a well-expressed transition in the rift zone direction from N–S to NE–SW, and so on [Mats et al., 2001].

A mantle plume is diagnosed here on the basis of gravimetric and seismological evidence [Zorin et al., 2003], and the crustal thickness is 40–41 km, while it is significantly smaller (34–35 km) in the Southern and Central basins [*Baikal …*, 1981]. According to data of deep seismic sounding in the NCBR, the seismic wave velocity beneath basins is smaller than beneath mountainous areas at the same depth levels. Moreover, a horizontal stratification of the crust is observed here at depths of 18–22 km, possibly indicating the presence of significant structural heterogeneities [Krylov et al., 1990].

The intensity and contrast of recent rifting movements in this part of the rift are recognizable from various types of seismic activity (Fig. 1). Apart from weak (background) and relatively strong ($M > 5.0$) events, earthquakes grouping into swarms or aftershock sequences are recorded here [Solonenko and Solonenko, 1987]. Stable tendencies in the seismic regime are reflected in the mosaic pattern of the epicentral field, the location of the majority of earthquake sources in the middle crust, and variations in the slope of the recurrence plot [Melnikova et al., 2003].

The study region experienced rather strong earthquakes in the 20th century. Thus, epicenters of two such events were localized on the basis of macroseismic evidence: the Lower Angara event (M = 5.9) of August 6, 1931, and the M = 5.3 earthquake of October 5, 1954 [*New Catalog …*, 1977] (Fig. 1). Only rare shocks with magnitudes $M \le 5.3$ were recorded in the NCBR in the period from 1954 through 1998. The strongest of them, the events of November 2, 1976 (M = 5.2) [Golenetskii, 1980], and October 26, 1990 ($MPSP$ = 5.3) [Golenetskii

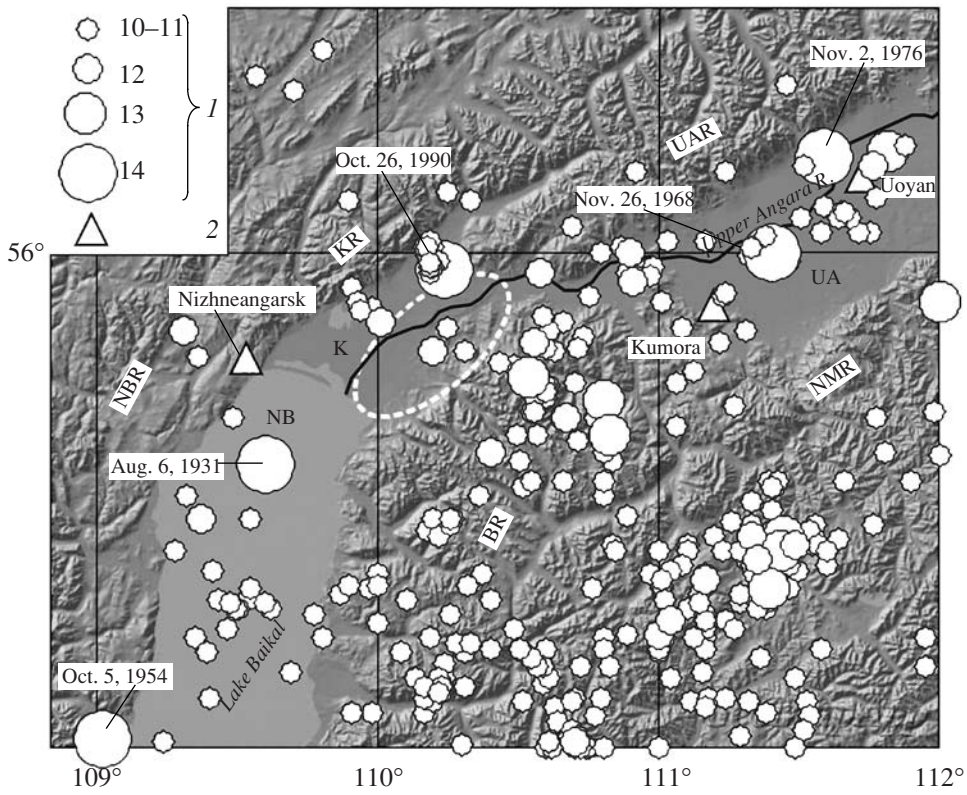

Fig. 1. Map showing the epicenters of NCBR earthquakes over the period 1931–1998: (*1*) energy classes (dates are shown for events with $K \geq 14$ or $Mw \geq 5.0$); (*2*) seismic stations. Rift basins: NB, Northern Baikal; K, Kichera; UA, Upper Angara. Uplifts: NBR, Northern Baikal Range; KR, Kichera Range; BR, Barguzin Range; UAR, Upper Angara Range; NMR, Northern Muya Range. The broken open line delineates the 1999 activation area.

et al., 1996], were followed by aftershocks and were located in the Kichera and Upper Angara basins. Earthquake swarms were recorded in mountainous areas of the Barguzin Range in this period (Fig. 1).

From the beginning of regular seismological observations (1960) up to 1999, a deficit in earthquakes was observed in the region between the northern termination of the Lake Baikal water area and the SE flank of the Kichera depression; this can be interpreted as evidence for seismic quiescence here. Two strong Kichera earthquakes ($Mw = 6.0$ and 5.6) spaced by a 1-min interval occurred on March 21, 1999, in the area of the interbasin mountainous isthmus between the Kichera depression and the Upper Angara basin (Fig. 2). They were preceded and followed by numerous shocks (more than 6000 from January through December 1999). By the number of events and the released total seismic energy, this sequence considerably exceeds all others known in the Cis-Baikal region. This provides a unique possibility for a detailed study of a large set of earthquakes: their spatiotemporal distribution, focal mechanisms, seismotectonic strain rates, and so on.

SEISMOTECTONIC CHARACTERIZATION OF THE NCBR

The main morphostructural elements in the area of the Kichera earthquakes are the Northern Baikal rift basin (with its northern termination on land; the Kichera depression), the Upper Angara rift basin; and the Northern Baikal, the Barguzin, the Upper Angara, and other ranges bounding these basins (Fig. 2). The negative rift structures are separated by the Kichera-Upper Angara interbasin mountainous isthmus, which includes the SW part of the Upper Angara arched block uplift complicated by the Dzelinda embryonic basin, the Takakonskaya intermediate step, and a part of the Barguzin arched block uplift. A wide (5–8 km) E–W trending grabenlike structure (merged satellite basins) crosses the interbasin isthmus. It is evident that the fault-block structure of the crust is best expressed in the area of the interbasin mountainous isthmus.

Basins of various types are controlled by active seismogenic rifting faults such as the Kichera, Dzelinda, and Upper Angara faults, as well as a fault bounding the Northern Baikal and Kichera rift basins to the southeast. Less active faults strike along the NE, E–W, and lateral (NW) directions.

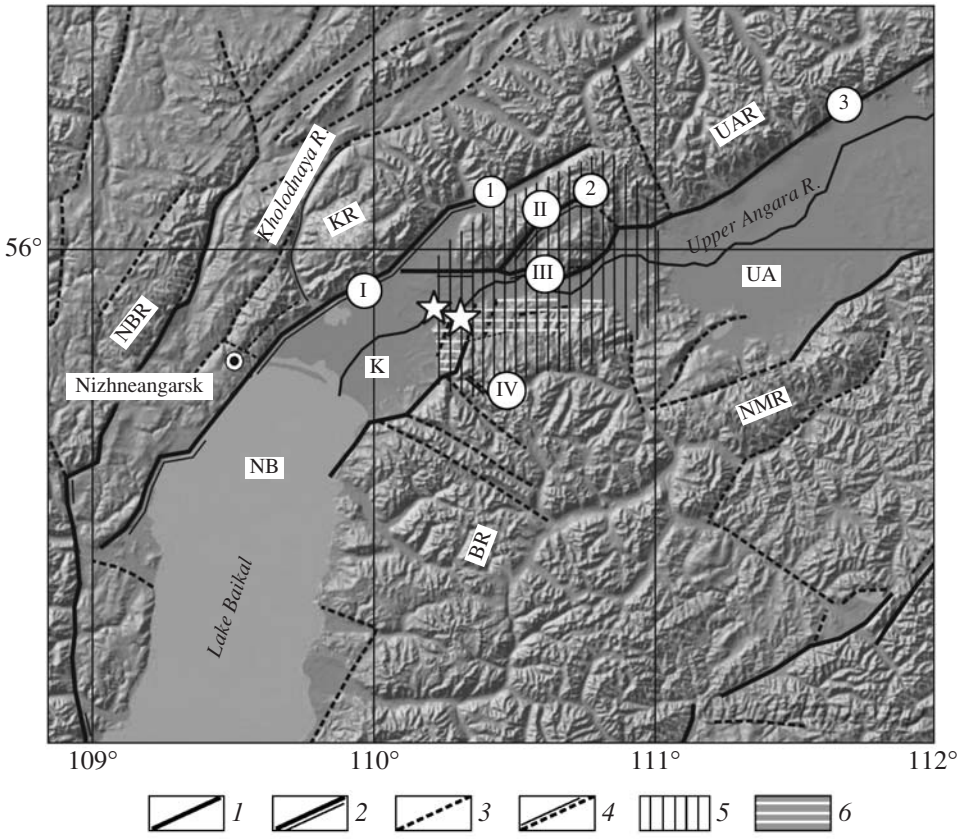

Fig. 2. Seismotectonic setting in the epicentral area of the Kichera earthquakes of 1999: (*1*) most active rifting faults (encircled numbers): (1) Kichera, (2) Dzelinda, and (3) Upper Angara; (*2*) paleoseismic ruptures in these fault zones (encircled Roman numerals): (I) Kichera, (II) Dzelinda, and (III) Ustdzelinda; (*3*) other neotectonic and supposedly active faults; (*4*) Krutaya paleoseismic rupture (IV) in the zone of such a fault; (*5*) Kichera-Upper Angara interbasin mountainous isthmus; (*6*) Takakonskaya intermediate step. The stars are epicenters of the strongest earthquakes of 1999. The designations of basins and ranges are the same as in Fig. 1.

The Kichera normal fault is one of the most active fractured structures within the NCBR. It is located on the NW flank of the Kichera basin, continuing the Lake Baikal basin. The Kichera fault is traceable over 150 km as a well-expressed scarp up to 1500 m in height coinciding with a thick bench [Lobachevskii and Golenetskii, 1979]. The maximum amplitude of displacements along the fault zone over the Cenozoic can reach 5.5 km. Seismotectonic movements have repeatedly occurred here in the Holocene, as is evident from offset alluvial fans of numerous rivers and creeks. Multiple seismotectonic scarps in the thickest alluvial fans reach 20–50 m in height. Single-event fault scarps of the Kichera paleoseismic deformation structure (PSDS) up to 6 m in height have been revealed in a 26-km segment of the fault considered [Khromovskikh et al., 1978].

A 50-m multiple scarp in the alluvial fan of the Kholodnaya River is divided into four constituent parts of different ages [Chipizubov and Stolpovskii, 2003]. The same pattern characterizes scarps in the Neruchanda River and other alluvial fans having displacement amplitudes of 6–7 m, which can indicate the occurrence in the past of earthquakes with magnitudes of 7.6–8.0. Deformations associated with the youngest paleoevent (a seismotectonic scarp slope of 38°–40°) took place no earlier than a thousand years ago. The length of ruptures of the next to last event, which occurred about three to four thousand years ago (scarp slopes of 32°–35°), supposedly amounted to ~60 km. The displacement amplitudes of the preceding paleoevent vary from 10 m (Neruchanda alluvial fan) to 30 m (Kholodnaya alluvial fan).

In the neotectonic structure, the Dzelinda fault bounds the steep NW flank of the Dzelinda embryonic basin; complicating the Kichera-Upper Angara interbasin mountainous isthmus. Seismotectonic deformations of the Dzelinda PSDS with vertical displacement amplitudes of up to 6 m have been established nearly all along this fault [Khromovskikh et al., 1978]. According to scale and preservation degree, the residual deformations in the Dzelinda basin also form a few systems of different ages. The youngest of them (no older than a thousand years) is seen in aerial photographs as a distinct thin line and is expressed in relief as well-preserved trenches and scarps traceable over 20 km. These

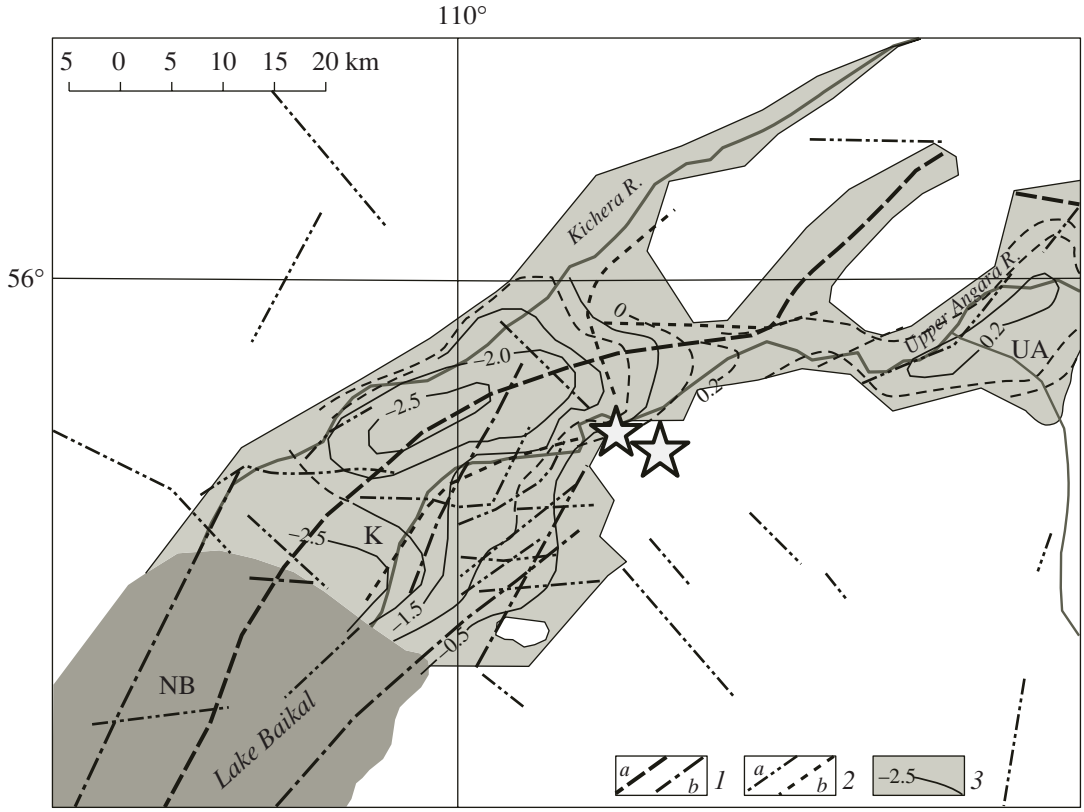

Fig. 3. Ruptures and other heterogeneities in the Kichera basin basement from geophysical data: (*1*) crush zones (*a*) and ruptures (*b*) from gravity data; (*2*) ruptures (*a*) and boundaries between blocks with different characteristics of the magnetic field (*b*) from aeromagnetic survey data; (*3*) Quaternary deposits filling rift basins and isohypses of the crystalline bottom of basins (elevations in km). Rift basins: NB, Northern Baikal; K, Kichera; UA, Upper Angara. The stars are epicenters of the strongest earthquakes of 1999. Data from [Pis'mennyi and Alakshin, 1980] were used for the construction of the scheme.

deformations are identical in characteristic features and morphology to deformations of the Yanchukanskaya and Kovoktinskaya peloseismogenic structures, northeast of the region under consideration, while tensile fractures are similar to those produced by the Muya earthquake of 1957, the strongest event in Eastern Siberia [*Seismotectonics* …, 1968].

In the neotectonic structure, the Upper Angara fault separates the rift basin and the uplift (ridge) of the same name. Two or three normal fault scarps with a total displacement amplitude of 2000–3000 m gradually decreasing northeastward are present here in a zone 2–3 km wide. No signature of the fault zone is observed in the gravity field, which indicates its Cenozoic age. The Ustzelinda paleoseismic rupture, extending for 4 km across the valley of the Dzelinda River at its confluence with the Upper Angara River, is present on the SW flank of the fault. Three faulting events are recognizable from Dzelinda River terraces and the steplike structure of a seismotectonic scarp 3 to 10–14 m in height. The last paleoevent had an amplitude of 2–3 m, and the two preceding had amplitudes of 5–6 m. A group of the Dzelinda thermal springs are located on the right-hand flank of the Dzelinda River valley near the base of a steep (33°–36°) multiple seismotectonic scarp up to 12 m in height. An extended (up to 1 km) band of thermal water (T = 36°C) outlets known under the name Goryachaya Kosa is traceable at the SW continuation of this scarp in the floodplain of the Upper Angara River.

The laser scanning of the Earth's surface carried out in 2005 revealed the presence of 7-km-long seismotectonic deformation features of the left-lateral faulting type. They are traceable along a line connecting the Kichera and Upper Angara faults (Fig. 2). The source of the relatively strong (*MPSP* = 5.3) earthquake of October 26, 1990, might have been associated with this structure.

The Krutaya paleoseismogenic structure is feature rather rare for the BRZ indicating young activation of NW trending faults (Fig. 2). Deformations of this structure are represented by a large rockfall (about 150 × 10^6 m^3 in volume) and a NW trending seismotectonic rupture 500 m long. Seismotectonic fractures are well expressed by reversed scarps 2 to 10 m in height (the mountainward wall of the fault is upthrown). The height of seismogenic scarps, largest at divide ridges, gradually decreases toward thalwegs of creek valleys, where seismotectonic dams are completely eroded.

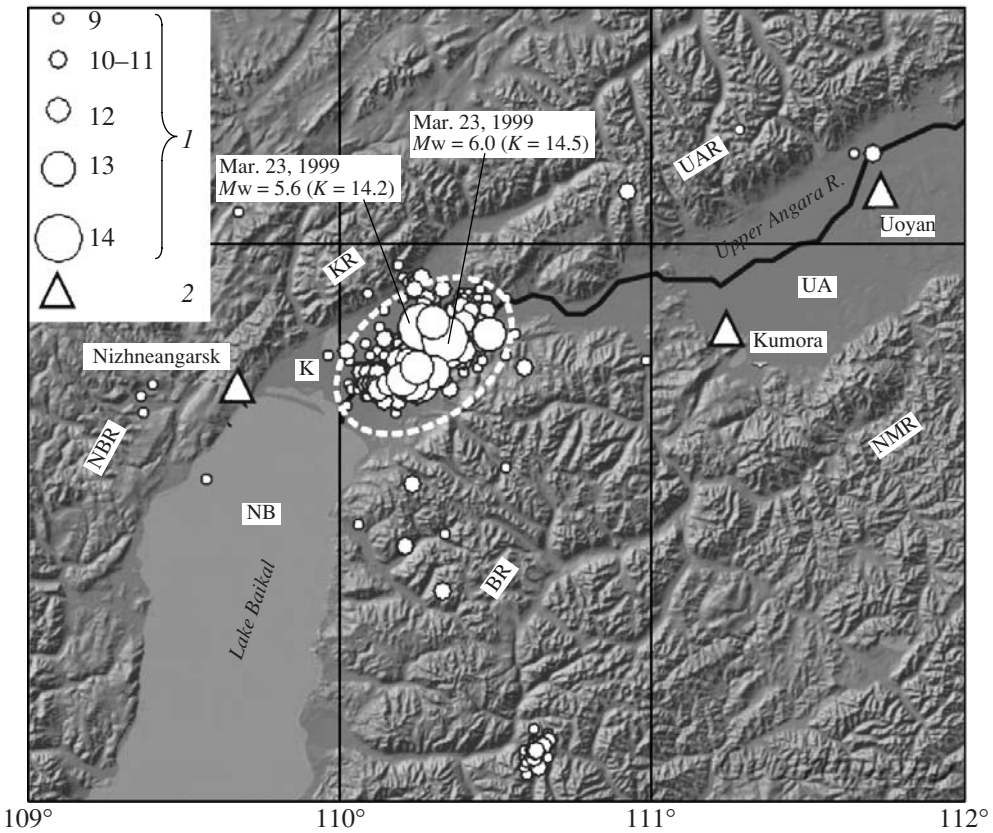

Fig. 4. Map showing earthquake epicenters of 1999: (*1*) energy class; (*2*) seismic stations. The broken open line delineates the localization area of the Kichera sequence of earthquakes (foreshocks, strong events, and aftershocks). Dates and energy classes are specified for the strongest shocks. The designations of basins and ranges are the same as in Fig. 1.

Ruptures penetrate basement granites and the overlying glacial deposits. The NW strike of the seismotectonic rupture with the upthrown SW mountainward wall can be regarded as evidence for a SW dip of the fault plane and, accordingly, reversed or reversed–strike-slip kinematics of the fault.

According to results of geophysical studies [Pis'mennyi and Alakshin, 1980], ruptures trending N–S, NE, and NW have been established in the basement of the Kichera depression (Fig. 3). One of the NW trending faults is present near the epicentral zone of the Kichera earthquakes; an interface between blocks differing in magnetic field characteristics that can have a fault origin is also fixed here.

Having considered the situation in the NCBR, we should note the following. Repeated seismotectonic activity pulses occurred here in the period of the neo-Baikal rifting activation. The presence of $M \leq 8.0$ paleoearthquakes (a few hundred to a few thousand years old) implies a high seismic potential of this part of the rift in the Holocene, while kinematics of fault zones suggests the predominance of the regime of extension oriented across structural faults.

DEVELOPMENT OF THE FOCAL ZONE OF THE KICHERA EARTHQUAKES OF MARCH 21 (Mw = 6.0 AND 5.6)

Although the majority of aftershocks occurred in the focal zone of the Kichera earthquakes (Mw = 6.0 and 5.6) by the end of 1999 (Fig. 4), seismic activity attenuated over a few years (Fig. 5).

Seismic events of 1999 were recorded by both analog and digital (Tyrgan, Irkutsk, Listvyanka, and Talaya) stations of the Baikal Branch of the GS SD RAS. The statistical error involved in the determination of epicentral coordinates of the study earthquakes mostly amounted to no more than 2–3 km for K = 10–14 events and up to 6 km for the others.

The HYPOINVERSE program [Klein, 1978] was used for localization of hypocenters. The following three conditions served as criteria for selection of earthquakes: records made at the two nearest stations are available, epicentral distances to at least three stations should not exceed 150 km, and no less than five pairs of distinct arrivals of *P*g and *Signal* waves can be identified in earthquake records. As a result, we considered about 800 seismic events whose hypocentral depth determination uncertainty did not exceed 5 km (Fig. 6).

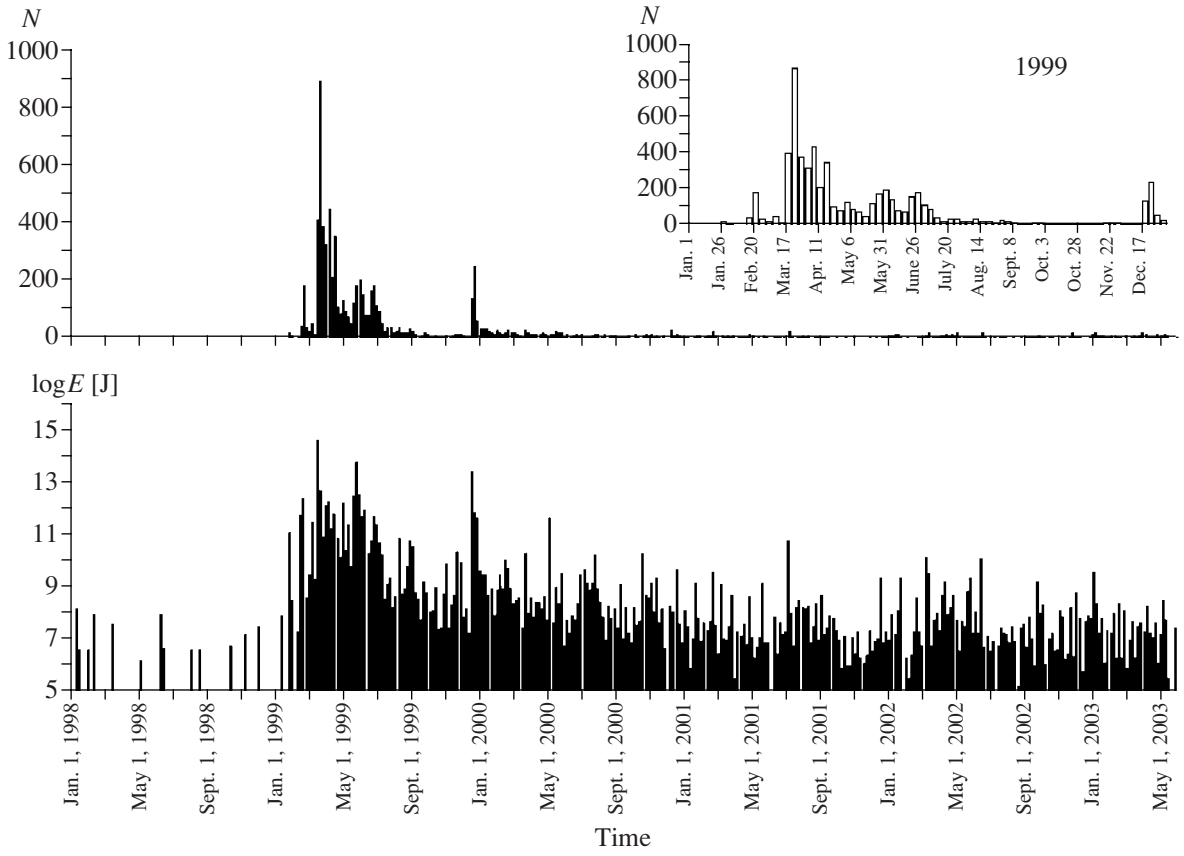

Fig. 5. Temporal variations in the number of earthquakes (*N*) and the logarithm of the total seismic energy (log*E*) of the Kichera sequence over the period from January 1, 1998, through June 30, 2003. The inset shows the distribution of earthquakes of 1999 (the scale division value of the abscissa axis is five days).

The absence of hypocenters at depths to 10 km (sections *AB* and *CD* in Fig. 6) is due to the fact that this limit was exceeded for smaller earthquakes.

With rms errors of determinations of arrival times being no more than 0.1 s, the average velocities had usual regional values: $V_p = 6.15$ km/s and $V_p/V_s = 1.73$. The depth distributions of hypocenters in the planes of sections *AB* and *CD* (Fig. 6) showed that they concentrate at depths of 16–30 km, although the entire crust is seismogenic in the epicentral zone, where its thickness amounts to 40–41 km according to deep seismic sounding data [*Baikal* …, 1981]. The seismically active crustal layer is distributed rather uniformly along the SE flank of the Kichera depression, slightly deepens toward the interbasin isthmus, and steeply dips NW.

RECURRENCE PLOT

Using the sufficiently representative data on the Kichera earthquakes, we determined the slope of the recurrence plot γ and analyzed its temporal behavior. The slope was calculated for several intervals of energy classes, and its values having the smallest error (usually within $\sigma_\gamma = \pm 0.03$) were selected. To check that the inferred patterns are not random, γ was estimated from successive samples consisting of 200 (first variant) and 400 (second variant) events.

The results of calculations presented in Fig. 7 show that γ amounted to -0.39 ± 0.01 during the foreshock activation period (before the 16:16 and 16:17 strong earthquakes of March 21). According to previous data obtained over the 30-yr observation period, the average absolute slope here is considerably larger: $\gamma = -0.53 \pm 0.001$ [Melnikova et al., 2003]. The smaller value of the recurrence plot slope is indirect evidence that the seismogenic volume of the crust was in a consolidated state before these shocks. The onset of the active aftershock process (from March 22 to April 1) was accompanied by an abrupt rise in the slope (up to $\gamma = -0.59$), indicating a partial release of accumulated stresses and a strength drop. In the next period, during April–May, the γ value gradually decreased and attained its initial level ($\gamma = -0.40$) at the time of the next strong ($K = 13.8$) shock of May 30. Afterward, a similar pattern was observed: the slope increased to $\gamma = -0.59$ over May–June and abruptly dropped a month before the earthquake of December 21 ($K = 13.5$), as seen from Fig. 7. Thus, the temporal variation in the recurrence plot slope provided constraints on the "fine" structure of accumulation and release of stresses during the seismic

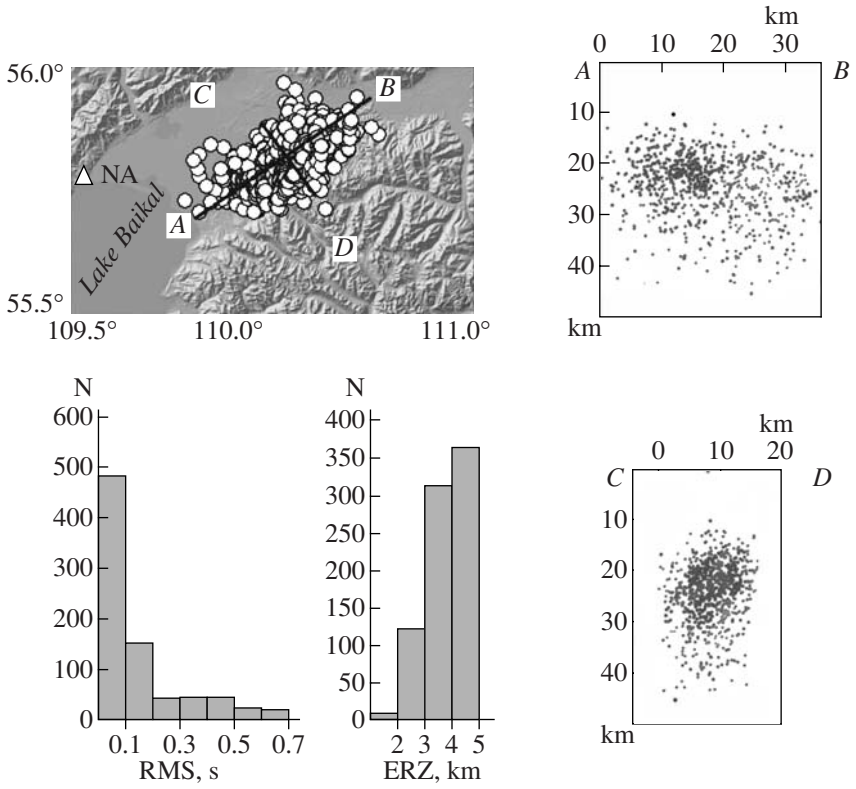

Fig. 6. Hypocenter distribution of the Kichera earthquakes of 1999 (the sections *AB* and *CD*) and their determination uncertainties (RMS and ERZ). Data for earthquakes with ERZ ≤ 5 km were used (see explanations in the text). The Nizhneangarsk seismic station is designated as NA.

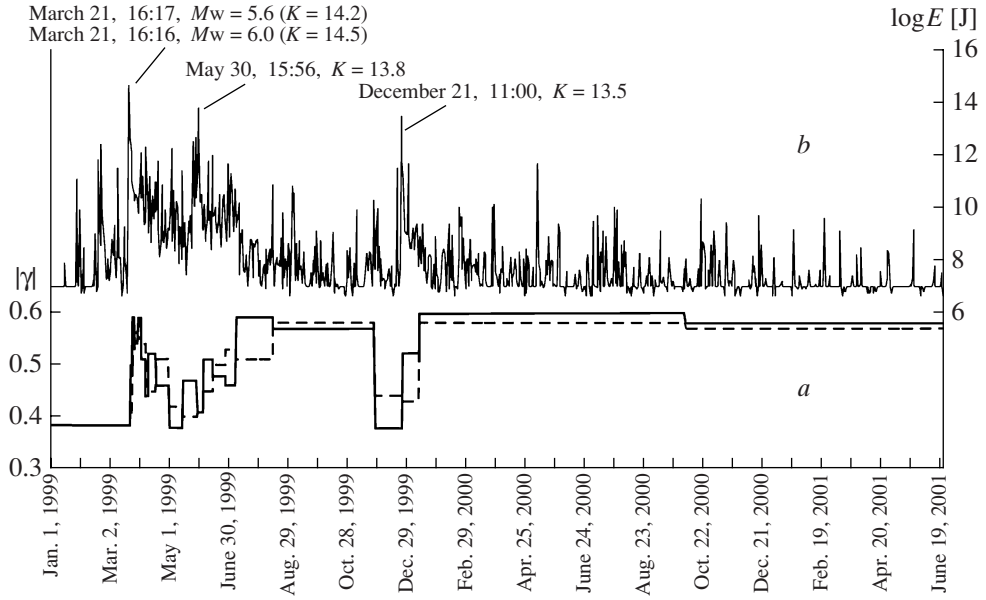

Fig. 7. (*a*) Temporal variations in the absolute slope value of the recurrence plot γ calculated from samples of $\Sigma N = 200$ events (solid line) and $\Sigma N = 400$ events (broken line) and (*b*) logarithm of the total seismic energy log*E*. The arrows show relatively strong earthquakes.

Table 1. Focal mechanisms of the Kichera earthquakes of 1999–2005

No.	Date	t_0	Epicenter		K	*MPSP*; *M*w	*NP*1, deg			Principal stress axes, deg							
			φ, °N	λ, °E			STK	DIP	SLIP	*T* pl	δ pl	*T* az	δ az	*P* pl	δ pl	*P* az	δ az
1	2	3	4	5	6	7	8	9	10	11	12	13	14	15	16	17	18
1	Feb. 18, 1999	02:11	55.79	110.40	10.9	4.3	3	38	172	38	0	336	0	30	0	219	0
2	Feb. 21, 1999	03:52	55.81	110.40	12.3	4.8	67	54	−62	5	0	138	0	67	0	35	0
3	″	15:48	55.84	110.37	10.6	4.2	3	42	−87	3	0	271	0	86	0	57	0
4	Mar. 21, 1999	16:16	55.83	110.34	14.5	5.8; 6.0	98	74	−38	13	13	153	1	38	9	53	8
5*	″	16:17	55.85	110.26	14.2	5.7; 5.6	50	47	−86	2		137		87		20	
6	″	16:42	55.82	110.34	11.4	5.7	152	42	−50	9	0	35	0	63	0	143	0
7	″	17:35	55.78	110.29	11.8	4.3	55	50	−76	4	5	135	2	79	8	24	41
8	″	19:40	55.80	110.34	11.3	4.3	293	70	55	52	12	162	4	17	14	48	11
9	″	20:29	55.81	110.32	10.3	4.5	276	64	−106	18	8	18	4	67	15	156	35
10	″	20:54	55.79	110.32	10.7	4.1	258	54	−63	5	4	329	6	68	29	226	16
11	″	22:00	55.77	110.32	11.1	4.2	194	49	−126	2	2	129	4	64	5	35	2
12	″	22:42	55.84	110.48	12.8	4.3	77	46	−90	1	2	167	19	89	2	347	11
13	Mar. 22, 1999	00:45	55.87	110.28	10.6	4.9	152	80	43	37	12	22	1	21	4	276	5
14	″	08:46	55.79	110.38	11.0	5.0	344	41	131	62	10	336	9	10	6	226	12
15	″	12:05	55.85	110.33	10.7	4.2	72	54	−110	7	0	176	0	72	0	288	0
16	″	12:29	55.77	110.30	12.6	4.2	6	42	−124	7	9	299	8	67	19	191	7
17	″	15:48	55.82	110.29	9.8	5.0	108	30	−41	22	3	343	8	58	6	113	11
18	Mar. 23, 1999	02:16	55.81	110.38	10.7	4.5	16	30	−90	15	13	286	8	75	14	106	48
19	″	12:03	55.86	110.39	10.7	4.3	72	58	−111	10	3	177	6	69	1	296	7
20	″	22:14	55.86	110.40	12.0	4.8	72	61	−83	16	0	157	0	73	0	359	0
21	Mar. 24, 1999	05:33	55.78	110.29	10.5	3.8	179	48	−105	2	2	280	6	79	1	20	47
22	″	19:22	55.85	110.30	10.4	4.0	269	86	−60	34	9	334	13	41	2	207	2
23	Mar. 25, 1999	01:32	55.83	110.47	10.6	4.3	4	40	−90	5	0	274	4	85	1	94	25
24	Apr. 1, 1999	00:23	55.88	110.42	10.9	4.7	72	76	−76	30	0	150	0	57	0	1	0
25	Apr. 2, 1999	16:39	55.78	110.27	12.1	5.0	80	50	−70	3	2	156	3	74	6	55	22
26	Apr. 7, 1999	08:37	55.75	110.25	11.3	4.5	48	64	−74	18	3	126	9	67	12	348	42
27	″	13:24	55.77	110.30	10.1	4.0	188	49	−108	3	1	291	16	76	14	31	48
28	Apr. 8, 1999	04:48	55.77	110.22	10.2	4.0	50	48	−77	2	2	131	6	80	9	29	3
29	Apr. 11, 1999	19:39	55.77	110.20	11.2	4.2	86	42	−72	4	1	343	24	77	9	92	16
30	Apr. 14, 1999	09:48	55.76	110.17	10.4	4.0	224	60	−94	15	15	317	4	75	10	123	54
31	Apr. 16, 1999	14:56	55.81	110.31	10.9	4.7	247	70	−87	25	8	335	18	65	7	162	15
32	Apr. 18, 1999	05:01	55.78	110.21	9.7	4.0	72	56	−98	11	2	168	10	77	5	315	35
33	Apr. 19, 1999	06:27	55.80	110.21	11.8	4.5	219	44	−86	1	4	126	21	87	6	234	69
34	Apr. 27, 1999	16:46	55.78	110.19	9.6	4.0	176	42	−74	4	1	75	6	79	8	186	31
35	May 2, 1999	01:29	55.77	110.17	10.0	4.0	56	50	−77	4	2	137	4	79	10	25	15
36	May 3, 1999	20:54	55.84	110.35	11.8	4.7	211	50	−84	5	4	297	19	83	10	158	25
37	May 5, 1999	09:20	55.83	110.29	10.6	4.5	335	44	−147	14	6	283	5	51	12	175	5
38	May 25, 1999	07:01	55.76	110.25	11.2	4.4	101	40	−99	6	0	18	0	82	0	245	0
39	″	13:21	55.76	110.25	12.5	5.0	247	60	−72	14	2	324	6	69	6	194	10
40	″	20:48	55.78	110.15	10.4	4.0	7	28	−144	25	7	316	3	55	1	183	16
41	May 27, 1999	16:01	55.76	110.20	12.7	5.1	245	56	−77	10	3	325	5	75	12	194	30
42	May 29, 1999	15:37	55.77	110.25	11.0	4.7	282	44	−62	4	2	173	4	71	2	275	10

Table 1. (Contd.)

1	2	3	4	5	6	7	8	9	10	11	12	13	14	15	16	17	18
43	May 30, 1999	15:56	55.76	110.25	13.8	5.6	186	43	−121	6	3	118	8	68	8	13	7
44	″	16:16	55.78	110.20	10.6	4.0	346	40	−136	13	12	288	8	59	19	175	8
45	May 31, 1999	19:34	55.75	110.23	12.6	4.6	240	72	−77	26	3	320	4	61	4	169	3
46	″	20:33	55.76	110.19	11.0	4.0	17	50	−110	3	2	121	12	74	14	222	23
47	June 2, 1999	12:51	55.77	110.28	10.2	4.0	67	80	−89	35	0	156	0	55	0	338	0
48	June 9, 1999	01:58	55.74	110.11	11.0	4.5	94	42	−79	4	3	356	4	82	8	111	29
49	″	03:00	55.74	110.13	11.6	4.8	77	54	−32	7	0	310	0	46	0	47	0
50	June 13, 1999	11:51	55.79	110.19	12.0	4.7	69	74	−64	25	8	139	5	54	3	10	18
51	June 14, 1999	02:10	55.79	110.18	9.5	4.0	58	44	−74	2	6	317	12	79	13	57	23
52	June 15, 1999	23:14	55.78	110.17	9.7	4.0	249	50	−86	5	5	336	2	84	6	190	6
53	June 20, 1999	15:49	55.72	110.14	10.5	4.0	43	50	−92	5	13	134	7	85	14	298	43
54	June 24, 1999	10:15	55.79	110.20	10.1	4.0	74	60	−63	11	3	145	23	64	5	31	55
55	July 4, 1999	20:57	55.74	110.13	10.2	4.0	110	32	−40	21	12	344	8	57	7	111	8
56	July 6, 1999	04:34	55.76	110.17	10.7	4.0	266	76	−104	30	10	8	6	57	11	157	10
57	July 10, 1999	16:02	55.76	110.19	10.2	4.0	352	42	−90	3	1	262	7	87	1	82	49
58	Aug. 13, 1999	08:55	55.75	110.17	10.9	4.0	256	26	−69	20	12	150	11	68	12	304	13
59	Sept. 2, 1999	16:04	55.75	110.08	10.8	4.0	344	42	−96	3	0	258	0	85	0	131	0
60	Sept. 4, 1999	12:03	55.75	110.08	10.5	4.0	180	50	−77	4	0	260	0	80	0	170	0
61	Nov. 6, 1999	01:48	55.75	110.16	9.9	4.4	66	50	−44	5	5	305	1	56	2	42	9
62	Dec. 21, 1999	11:00	55.78	110.25	13.5	5.8	56	60	−118	11	1	166	9	63	1	278	9
63	Dec. 22, 1999	01:39	55.74	110.21	11.6	4.7	216	46	−76	0	4	116	8	80	9	206	39
64	Dec. 23, 1999	22:24	55.75	110.26	11.1	4.6	207	60	−94	15	12	300	3	74	10	105	56
65	Feb. 18, 2000	15:09	55.74	110.32	10.0	4.2	92	44	−90	1	1	2	1	89	2	182	38
66	June 8, 2000	20:40	55.63	110.12	9.8	4.4	70	60	−56	9	2	136	4	60	4	30	4
67	July 5, 2001	07:10	55.89	110.29	10.4	4.1	73	60	−60	9	3	141	6	63	6	33	5
68	Mar. 7, 2002	07:55	55.74	110.23	10.0	4.4	229	86	−50	29	10	288	7	36	6	173	2
69	″	08:11	55.76	110.22	9.7	4.4	325	49	−117	1	2	73	3	70	2	165	10
70	Mar. 11, 2002	16:53	55.75	110.23	9.5	4.3	50	70	−50	15	0	112	0	49	0	3	0
71	Dec. 31, 2002	01:08	55.88	110.45	9.6	4.2	68	56	−50	3	0	131	0	58	0	37	0
72	May 5, 2004	17:46	55.74	110.25	10.9	4.6	39	44	−61	5	0	289	0	69	0	31	0
73	Mar. 20, 2005	06:04	55.81	110.23	9.8	4.2	220	24	−112	22	5	146	3	66	4	349	4
74	Apr. 14, 2005	15:40	55.80	110.10	10.1	4.4	72	56	−44	1	0	131	0	53	0	40	0
75	Apr. 29, 2005	00:31	55.79	110.09	10.1	4.4	64	54	−47	0	0	125	0	56	0	35	0
76	May 6, 2005	03:09	55.76	110.13	10.2	4.4	196	56	−86	11	6	283	11	79	8	120	26

Note: The magnitudes *MPSP* and *M*w are given after MOS and NEIC data, respectively. *NP*1 is a nodal plane; *T* and *P* are the extension and compression axes, respectively; and δ pl is the determination uncertainty. The asterisks indicate solutions obtained by the centroid moment tensor method (HRVD data).

activation of 1999 and the lengths of crustal strengthening and weakening time intervals.

FOCAL MECHANISMS AND SPATIOTEMPORAL DESTRUCTION OF THE CRUST

The focal mechanisms of the Kichera earthquakes were determined by the standard technique from first arrival signs of the longitudinal waves *P*n and *P*g. The accuracy of the resulting solutions (Table 1) was estimated from the limits of variations in dip angles of the principal stress axes (compressive, tensile, and intermediate).

The chain of interrelated seismic events in the area of the Kichera-Upper Angara interbasin isthmus started to form approximately two months before the two strongest earthquakes. The area of the initial (foreshock) activation was distinguished by a compact and

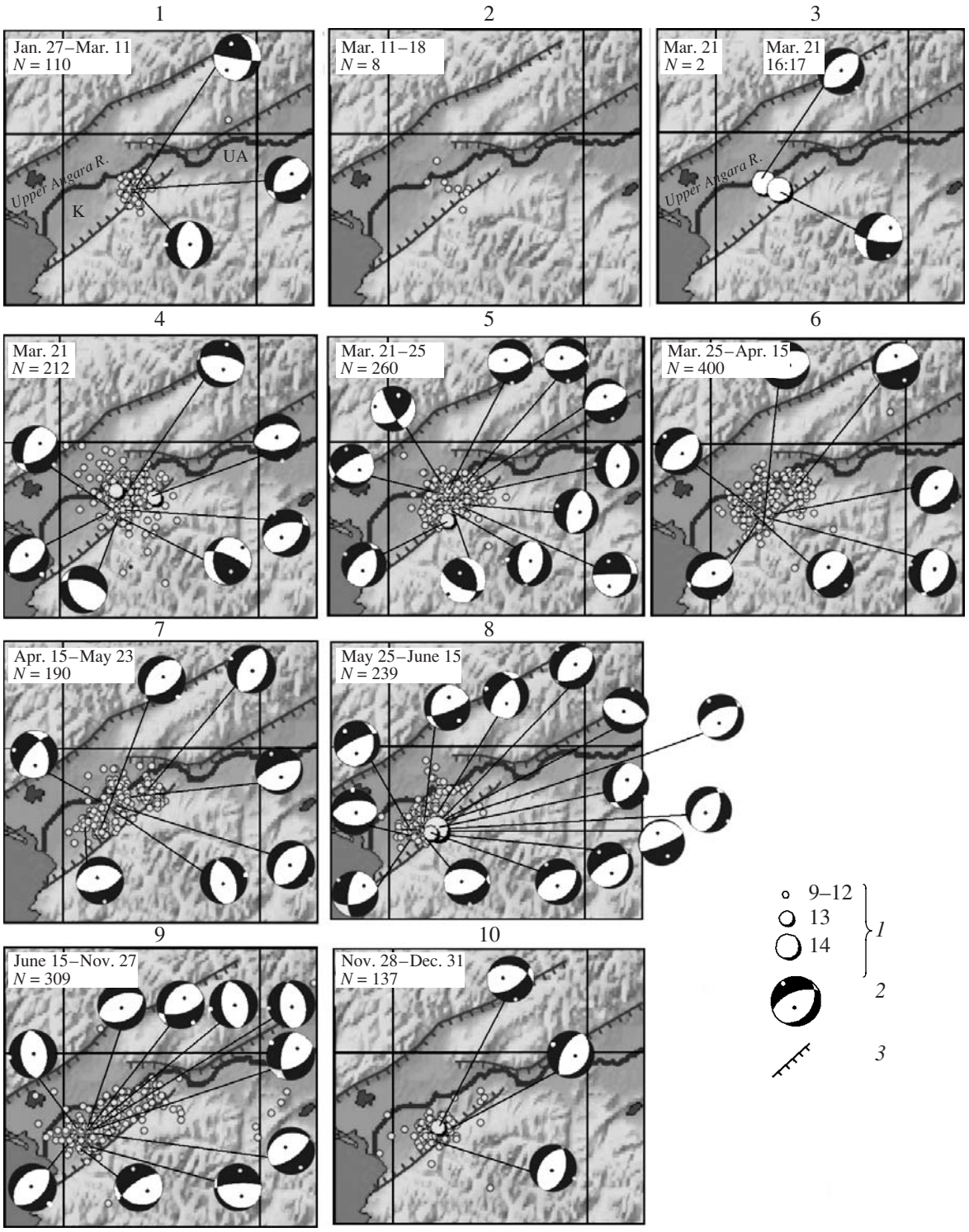

Fig. 8. Ten maps (1–10) showing epicenters of the Kichera earthquakes (foreshocks, strong events, and aftershocks) for various time intervals (the overall period is January 27–December 31, 1999): (*1*) energy classes of earthquakes; (*2*) focal mechanisms in the projection onto the lower hemisphere (compression areas are shaded, and dates and times are specified for the strongest events); (*3*) Cenozoic normal faults. Observation time intervals and numbers of events are shown in the upper left corners of panels. The designations of basins are the same as in Fig. 1.

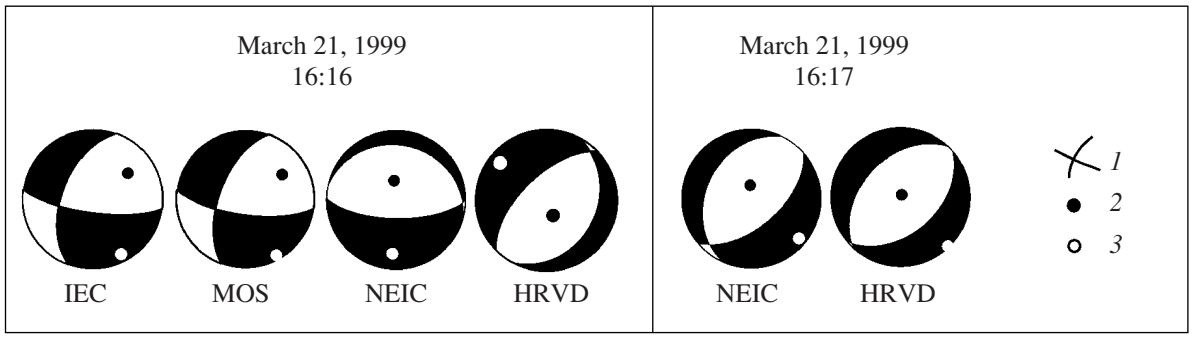

Fig. 9. Focal mechanisms (projections onto the lower hemisphere) of two Kichera earthquakes (Mw = 6.0 and 5.6) from IEC (Irkutsk), MOS (GS RAS, Obninsk), NEIC (USGS, National Earthquake Information Center) and HRVD (Harvard University, Centroid Moment Tensor Catalog data): (*1*) nodal lines; (*2, 3*) axes of principal stresses of (*2*) compression and (*3*) extension. Areas of compressional waves are shaded.

isometric shape, and motions in the sources were of the normal and strike-slip types (Fig. 8.1). Only a few weak ($K \le 9$) earthquakes were recorded in the epicentral zone of the future main shocks during the ten days before their occurrence (Figs. 8.2, 8.3).

According to data of various seismological agencies, the focal mechanism of the first strong shock (March 21, 16:16; Mw = 6.0) had four solutions obtained from both P wave first arrival signs and by the centroid moment tensor method (Fig. 9). The IEC and MOS solutions yielded a significant strike-slip component in fault planes trending N–S and E–W, while normal motions took place on E–W and NE trending fault planes according to the NEIC and HRVD solutions. As regards the focal mechanism of the second strong shock (March 21, 16:17; Mw = 5.6), it was very typical of a rift: both nodal planes trended NE and were characterized by normal faulting.

Because a few fault plane solutions were obtained for the first strong shock and only one focal mechanism was obtained for the second strong shock, the development of rupturing processes can be interpreted in two ways: (1) the initial displacement (of the strike-slip type in the first source) occurred in the E–W plane, which was followed by motions of the normal type on the NE trending plane, or (2) an initial normal motion in the first source occurred on the NE trending fault plane (HRVD) and the kinematics in the second source was similar.

The first interpretation is supported by the NW–SE orientation of the elongated epicentral field of a few weak foreshocks (Fig. 8.2) and the geometry of the epicentral field of aftershocks that occurred during the first day after the strong earthquakes (Fig. 8.4). As noted above, NW and E–W ruptures are present in the complex structure of the interbasin mountainous isthmus where the earthquakes in question were localized. Another example of this situation is the Krutaya paleoseismogenic structure, reflecting young activation of a NW striking fault.

Since the spatial coordinates of both events are close, the first scenario of faulting implies that stresses were released on intersecting faults striking NW (the first shock) and NE (the second shock); this does not contradict general laws of the formation and configuration of systems of conjugate faults developing due to fracture of rocks. The possibility of successive movements on such structural faults was substantiated by physical simulation studies [Ma Tzin et al., 2000].

The second variant of the source region development is simpler: the plane striking NE and dipping NW is chosen as an active plane in both sources. This assumption agrees well with the fact that both strong earthquakes are genetically related to the general NE-trending rifting fault, bounding the SE flank of the Kichera basin; this is confirmed by the spatial distribution of aftershock hypocenters, delineating the source zone of the strong shocks (Fig. 6).

The configuration of the epicentral field and focal mechanisms of some aftershocks indicate that both NE and NW or E–W faults were involved in the activation (Figs. 8.4–8.10). According to geological evidence, the two latter types of crustal destruction have produced structures of second order [Sherman et al., 1992]. A rapid change in the orientation of the epicentral field from NW to NE (Figs. 8.4–8.6) suggests activation of conjugate faults. Since 1999, the crustal stress release rate in the study region has dropped and earthquake sources have been of the normal and normal–strike-slip faulting types (Table 1).

SEISMOTECTONIC DEFORMATIONS

According to geological and geophysical data, the NCBR crust has been subjected to NW–SE extension throughout the rifting period [Solonenko et al., 1993; Levi et al., 1996; Melnikova and Radziminovich, 1998]. This conclusion is based on a large volume of data including rupture parameters directly established from geological outcrops and catalogs of focal mecha-

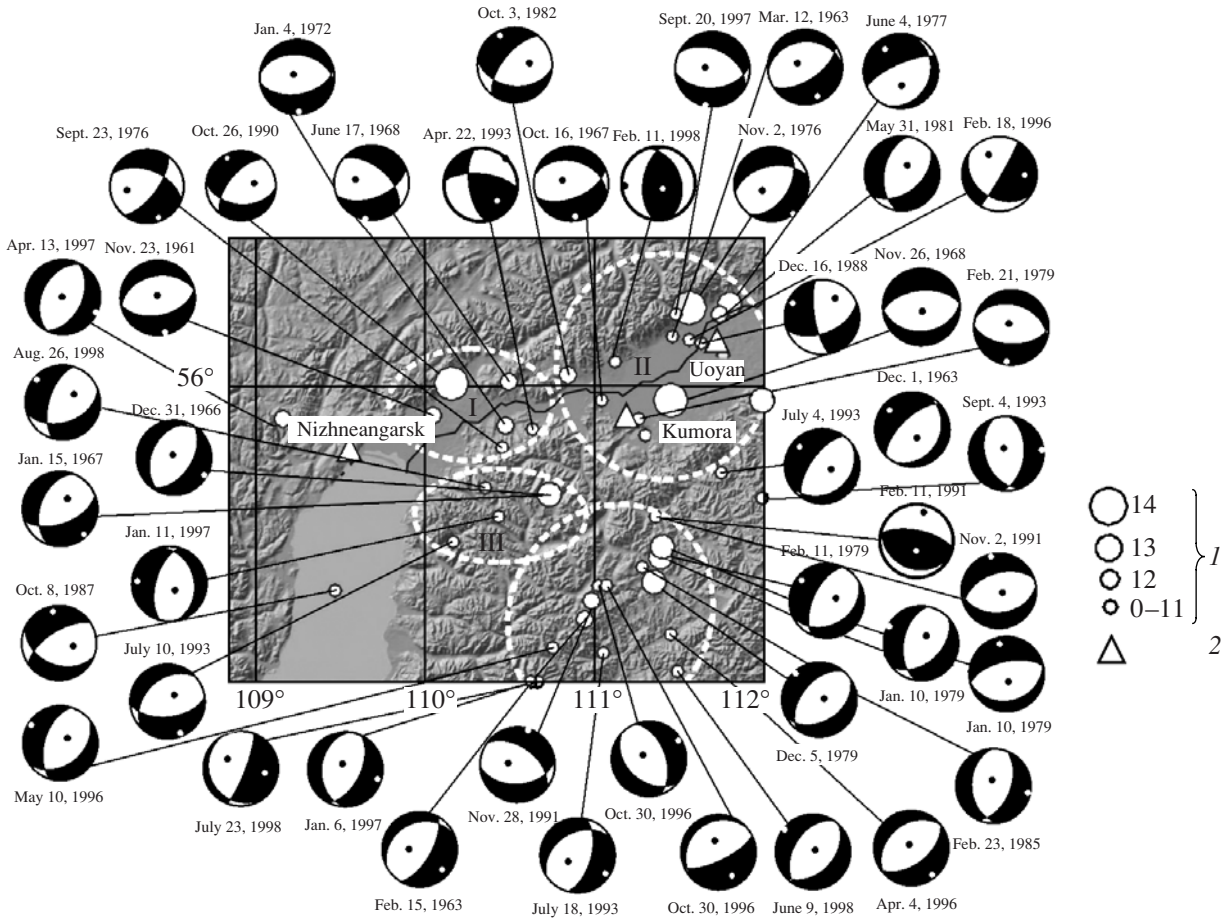

Fig. 10. Focal mechanisms (projections onto the lower hemisphere) of NCBR earthquakes (before 1999): (*1*) energy classes; (*2*) seismic stations. The open dashed lines delineate seismically active areas: (I) Kichera basin; (II) Upper Angara; (III, IV) northern (III) and central (IV) parts of the Barguzin Range.

nisms. Statistical analysis of focal mechanisms provides a basis for the principles of reconstructing seismotectonic deformations (STDs); these principles have been elaborated over the last decades and have been widely applied in studies of deformation processes in various seismically active regions [Riznichenko, 1977; Yunga, 1990, 1999; Sycheva et al., 2005].

The ideas of a seismic flow of rock masses [Riznichenko, 1977] or a mean mechanism of earthquakes [Yunga, 1990] are invoked to describe the deformation mechanism in a seismically active crustal volume due to fault motions in earthquake sources. Since both approaches to the estimation of the stress–strain state of the crust have been repeatedly discussed in the literature [Yunga, 1990; Sycheva et al., 2005], we mention here only their main distinctions. They consist in the fact that various focal mechanisms can be used for calculating parameters of a seismic flow of rock masses, whereas the determination of a mean mechanism requires that individual fault plane solutions be similar. Although these methods are based on different systems of assumptions, they complement each other, and, as a result, STD can be considered against the seismic flow.

In the general case, the seismotectonic strain rate is given by the formula [Yunga, 1990]

$$\langle \varepsilon_{ij} \rangle = \frac{1}{\mu VT} \sum_{n=1}^{N} M_0^{(n)} m_{ij}^n, \qquad (1)$$

where μ is the shear modulus, V is the averaging volume, T is time, m_{ij} is the directing tensor of the seismic moment of an nth earthquake, and $M_0^{(n)}$ is the value of the seismic moment of an earthquake ($n = 1, 2, \ldots, N$) determining its energy contribution to the STD. In the case of weak and moderate earthquakes, the seismic moment is usually determined from its correlation dependence on the energy class or the magnitude.

In the Cis-Baikal region, where the majority of fault plane solutions are very similar, deformation parameters are calculated using the idea of a mean focal mechanism as a particular modification of the notion of a seismic flow of rock masses. Using as a weight the

Table 2. STD parameters for the NCBR crust

Areas	Nodal point coordinates		*T*		*P*		χ	μ	ω	ρ	*N*
	φ, °N	λ, °E	Az	Pl	Az	Pl					
1961–1998											
Kichera basin	55.85	110.15	163	7	277	73	0.74	–0.41	134	16	6
Upper Angara basin	56.17	111.76	152	0	254	89	0.60	–0.06	152	1	13
Northern Barguzin Range	55.60	110.80	309	2	46	73	0.88	–0.12	149	19	5
Central Barguzin Range	55.20	111.00	132	6	342	83	0.72	–0.22	157	12	19
1999											
Kichera basin	55.79	110.40	317	2	143	88	0.70	–0.21	157	5	61
2000–2005											
Kichera basin	55.79	110.40	300	1	33	71	0.78	–0.10	147	20	12

Note: *T* and *P* are the principal axes of extension and compression, respectively; χ is the coefficient of agreement between individual and average mechanisms; μ is the Lode–Nadai coefficient; *N* is the number of fault plane solutions; ω is the angle of the stress state type; and ρ is the parameter of the angular relationship between motions on the horizontal and vertical planes.

weight function presented in [Yunga, 1990, 1999; Sycheva et al., 2005], the tensor of the average STD rate takes the form

$$\langle \varepsilon_{ij} \rangle = \frac{1}{\mu VT} \sum_{n=1}^{N} M_0^{(n)} \sum_{n=1}^{N} w^{(n)} m_{ij}^{(n)} / \sum_{n=1}^{N} w^{(n)}, \qquad (2)$$

where $w^{(n)}$ is the weight function, the inner sum is the matrix of the average mechanism, and the outer sum is taken over seismic moments in the seismically active crustal volume under consideration.

The mean mechanism is graphically represented by the surface of an elliptic cone whose shape and position are given by the orientation of principal axes of tensile (*T*), intermediate (*B*), and compressive (*P*) strains corresponding to the eigenvalues M_1, M_2, and M_3 ($M_1 < M_2 < M_3$) of a symmetric tensor of second rank and by the Lode–Nadai coefficient μ. The degree of consistency of the used data χ is estimated as the generalized measure of similarity of each event with respect to the average tensor [Yunga, 1990].

The stress–strain state of a seismogenic crustal layer 20 km thick (in the period from 1961 through 1998) was reconstructed for four seismically active regions: the Kichera depression, the Upper Angara basin, and the northern and central parts of the Barguzin Range (Fig. 10). The sought values were then obtained for the Kichera depression over the periods of 1999 and 2000–2005. The coordinates of nodal points (centers of regions) and the resulting values of STD parameters are presented in Table 2, and the stereograms of focal mechanisms are shown in Fig. 11.

The energy representativeness of earthquakes ($K \geq 9.5$ and $M \geq 3.0$) whose mechanisms were used for calculating the STD intensity and direction raises no doubts and, therefore, these data can be regarded as describing correctly enough the stress–strain state of the medium on the chosen space–time scales (Figs. 8, 10; Table 1). Note that variously directed structural faults were activated on the territory under study before 1999, while only E–W trending faults were activated in 1999 and in the subsequent period (Fig. 11).

The calculations showed a high degree of agreement between individual and resulting mechanisms in seismically active regions ($\chi \geq 0.60$): the extension axis *T* is invariably subhorizontal and oriented NW–SE, whereas the compression axis *P* is subvertical and has a significant scatter in azimuth values (Table 2). The values of the Lode–Nadai coefficient μ characterizing the type of the strain state indicate the predominance of tensile and shear deformations in the NCBR crust.

In addition to the characteristics of the complete matrix of the mean mechanism, Table 2 presents the components responsible for the generalized plane and shear deformations of the seismically active crustal layer [Yunga, 1999]. The generalized plane strain component is described by the parameter ω, the angle of the stress state type. In the given case, its values ($134 \leq \omega \leq 157$) correspond to the extension regime [Yunga, 1999; Sycheva et al., 2005]. The angular parameter ρ provides constraints on the relation between the generalized plane and shear strains. The smaller its value, the closer the crustal stress state to generalized plane deformation.

In calculating the average STD rates, two variants of weight coefficients were considered: (1) the seismic moment [Riznichenko, 1977] and (2) the weight function [Yunga, 1999]. As a result, we found that the values of the normal components (ε_{xx}, ε_{yy}, ε_{zz}) of the mean strain rate tensor (with various weight coefficients) are close to each other (Table 3). Certain divergences, occasionally rather significant, are observed in strain values and sign (compression or extension) along the direc-

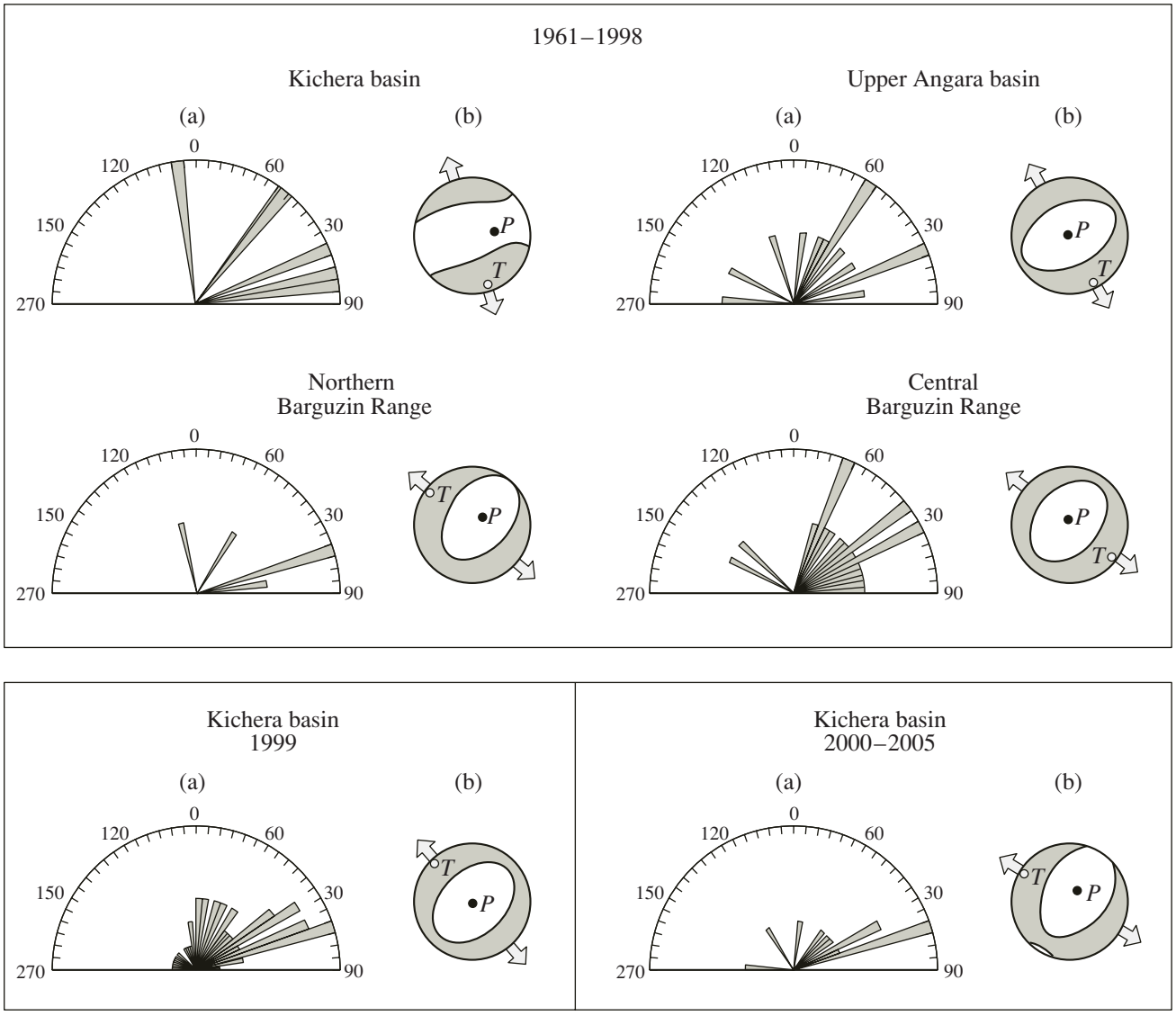

Fig. 11. Diagrams showing fault plane strikes in earthquake sources (a) and stereograms of average focal mechanisms (b) in four NCBR areas (see Fig. 10). The divergent arrows show the predominant deformation regime (NW–SE horizontal crustal extension). *P* and *T* are the principal axes of compression and extension, respectively.

tions of shear components (ε_{xy}, ε_{yz}). Table 3 shows that, if the energy level of Cis-Baikal earthquakes does not exceed $K = 14$, the use of different weight coefficients does not change significantly the results of calculations.

Thus, in the period 1961–1998, the average STD rates in the Kichera and Upper Angara basins were one to two orders higher than in mountainous areas of the Barguzin Range. In the Kichera basin, nearly all components of the strain rate tensor rose by two orders of magnitude at the time of seismic activation of 1999 and abruptly dropped by three orders in 2000–2005 (even by four orders in the case of the vertical component ε_{zz}). The energy potential of the seismic process in the basin decreased rather rapidly (over six years) to a level typical of the NCBR [Melnikova et al., 2005].

Seismological methods of observations of crustal deformations are not the only methods providing constraints on activation processes in the tectonosphere; in this respect, geodetic data of surface GPS measurements increase the amount of pertinent information and improve its quality. Preliminary comparison of both groups of data obtained for central and southwestern parts of the Baikal rift showed that recent tectonic movements and average STD rates differ by about an order of magnitude. At present, GPS sites are absent in the region under consideration, but STD rate values are comparable with those in the southern Baikal area [Radziminovich et al., 2005]. The contribution of the seismic component to the total deformation in the NCBR is approximately the same as in other parts of the rift.

Table 3. Components of the STD rate tensor for seismically active blocks of the NCBR crust

Areas	V, km^3	T, years	$\langle\varepsilon_{ij}\rangle \times 10^{-10}$ yr^{-1}						References
			ε_{xx}	ε_{yy}	ε_{zz}	ε_{xy}	ε_{yz}	ε_{zx}	
1961–1998									
Kichera basin, K = 10.2–14.0	28478	33	–4.11	41.50	–37.39	–46.32	6.08	–51.74	[1]
			–8.04	38.97	–30.94	–29.74	–14.29	–16.51	[2]
Upper Angara basin, K = 9.7–14.0	75035	36	4.69	23.63	–28.33	–21.61	20.71	4.92	[1]
			4.79	15.29	–20.09	–15.31	–0.06	1.09	[2]
Northern Barguzin Range, K = 10.2–13.0	22172	33	2.74	2.70	–5.44	–8.36	–5.65	–2.46	[1]
			3.45	2.39	–5.83	–5.93	–2.52	–3.14	[2]
Central Barguzin Range, K = 9.6–13.0	89784	36	2.02	3.05	–5.08	–3.75	0.66	–1.28	[1]
			2.32	2.10	–4.42	–3.25	–1.64	0.77	[2]
1999									
Kichera basin (all available focal mechanisms are used), K = 9.5–14.5 (Mw ≤ 6.0)	15888	1	2322	6336	–8654	–15 631	–10 917	–2054	[1]
			4856	5579	–10 435	–8183	827	–1209	[2]
Kichera basin (without focal mechanisms of the two strongest events), K = 9.5–13.8	15888	1	1542	1509	–3051	–2654	–1273	696	[1]
			1272	1433	–2705	–2025	344.73	–305.81	[2]
2000–2005									
Kichera basin, K = 9.5–10.9	18520	6	0.96	0.22	–1.19	–1.16	–0.69	–0.64	[1]
			0.84	0.26	–1.09	–1.07	–0.67	–0.47	[2]

Note: Boundaries of the areas are shown in Fig. 10. V is the seismically active volume and T is the time period. The STD rate components $\langle\varepsilon_{ij}\rangle$ are given in the coordinate system (X, east; Y, north; Z, up). The calculations used methods proposed in [1] (Riznichenko, 1977) and [2] (Yunga, 1999) (the References column).

DISCUSSION

The seismotectonic regime of NW–SE extension in the NCBR crust has persisted for a long time on the geological time scale because it has not experienced any significant changes during the Holocene. On the other hand, the recent and short-term components of deformation processes (from a few days to tens of years) depend on regional and local structural features of the crust (its geological and geophysical characteristics). The two latter types of seismotectonic relationships had direct implications for the Kichera earthquakes.

It is common knowledge that, according to some researchers, the BRZ is developing through the growth of basins and the subsidence of some parts of ranges and mountainous isthmuses. Thus, R.A. Kurushin and S.D. Khilko wrote that "… the SW termination of the Upper Angara basin is differentiated in a complex manner. Here there exist both negative and positive morphostructures of second rank. Both types are involved in the overall recent subsidence of the SW termination of the basin, indicating its longitudinal growth at the expense of the mountainous isthmus between the Upper Angara and Kichera basins" [*Seismotectonics …,* 1968, p. 156]. The study of the Kichera earthquake sequence provided convincing arguments in favor of the above suggestions. The crustal destruction process, starting in the area of the interbasin mountainous isthmus, propagated along the SE flank of the Kichera depression, without affecting its bounding mountainous areas, to the southwest toward the Baikal water area. The entire seismically active volume seems to be locked between the SE flank of the depression and the Upper Angara channel.

A large NE-trending fault (continuing the Upper Angara fault) controlling the rift and bounding the Kichera depression to the southeast played a decisive role in the realization of the above events. This is supported by the focal mechanism of the strongest shocks and the majority of aftershocks whose fault planes strike NE and dip NW. E–W, NW, and N–S structural faults were activated in fewer sources (Fig. 11).

It is evident that the energy potential and the large number of Kichera earthquakes were predetermined by the complex fault-block structure of the interbasin mountainous isthmus area. The presence of structural heterogeneities in the source zone was also substantiated by geophysical data: anomalously low velocities, the position of the mantle surface, and so on [Krylov et al., 1990].

Local crustal heterogeneities are likely to have controlled the stress release type and to be responsible for

grouping of the Kichera events, but processes of a larger scale level could have played the role of a trigger mechanism. It is known that the seismic regime in the BRZ in 1999 was not ordinary [Melnikova et al., 2005]. Apart from the Northern Baikal region, the Southern Baikal region was also distinguished by exceptionally high seismic activity. Overall, the Kichera and Southern Baikal earthquakes accounted for nearly all of the seismic energy released in the Baikal region over the year, and the total amount of $K \geq 5$ events exceeded 10 000. Note that the stress release of a similar type was observed in the crust of the NE flank of the BRZ (the Oldongsinskii swarm) [Radziminovich et al., 2004]. All this indicates that the aforementioned activations were due to a common mechanism favorable for the stress release precisely in crustal zones liable to fractures of such a type. This mechanism could have been due to the interaction between the external dynamic forces caused by movements of lithospheric plates and the local geodynamic processes accommodating the rise of anomalous mantle toward the base of the crust.

CONCLUSIONS

The Kichera sequence of earthquakes of 1999 confirmed the high seismic potential of the Northern Cis-Baikal region established from geological survey and seismogeological data. A detailed study of this seismic activation has led to the following conclusions.

(1) The rupturing process started within the Kichera-Upper Angara interbasin mountainous isthmus, where the fault-block structure of the crust is best developed, and propagated in the SW direction.

(2) Destruction of the crust was local and was controlled by a seismogenic rifting fault trending NE and bounding the Kichera depression to the southeast.

(3) The stress release pattern in seismic sources was consistent with the fault kinematics established from geological and geophysical evidence and pointed to active normal faulting beneficial to the longitudinal growth of the Upper Angara basin and deepening of the Kichera depression.

(4) The values of the seismotectonic strain rate calculated for the seismically active Northern Cis-Baikal region before and after 1999 lie within the range 10^{-9}–10^{-10} yr^{-1} (being higher in basins as compared with ridges), which is one to two orders smaller than the values obtained from geodetic data for the central and southern rift segments. The rates increased to 10^{-6}–10^{-7} yr^{-1} in 1999 and were highest along the directions of the vertical (ε_{zz}) and shear (ε_{yz}) components of the average strain rate tensor.

Thus, our study showed that the recent development of the Northern Cis-Baikal region (within the limits of the area considered) has been realized through growth of basins and destruction of interbasin mountainous isthmuses. The joint analysis of the obtained seismogeological information and geological and geophysical data provided deeper insights into the development of seismicity in the Cis-Baikal region and unbiased constraints on seismic hazard potential in the territory studied.

ACKNOWLEDGMENTS

This work was supported by the Russian Foundation for Basic Research, project nos. 06-05-64148 and 05-022-97285; the SD RAS Integration Project (no. 87); and the RAS Presidium Program 16, project 3.

We are grateful to the GS Baikal Branch, SD RAS, which provided us with records of digital seismic stations; we also thank R.A. Kurushin and L.P. Imaeva for discussion and valuable comments.

REFERENCES

1. *Baikal Interiors from Seismic Data* (Nauka SO, Novosibirsk, 1981) [in Russian].
2. A. V. Chipizubov and A. V. Stolpovskii, "Identification of Single-Event Paleoseismic Ruptures in the Kichera and Paramskii Fault Zones," in *Stress–Strain State and Seismicity of the Lithosphere* (SO RAN Filial "Geo," Novosibirsk, 2003), pp. 474–478 [in Russian].
3. S. I. Golenetskii, "Earthquakes of the Cis-Baikal Region," in *Earthquakes of 1976 in the USSR* (Nauka, Moscow, 1980), pp. 46–57 [in Russian].
4. S. I. Golenetskii, O. V. Belousov, G. F. Drennova, et al., "The Northern Baikal Earthquake of October 26 (27), 1990," in *Earthquakes of 1990 in the USSR* (OIFZ RAN, Moscow, 1996), pp. 67–71 [in Russian].
5. V. S. Khromovskikh, V. P. Solonenko, A. V. Chipizubov, and V. M. Zhilkin, "Seismotectonic Characterization of the Northern Cis-Baikal Region," in *Seismicity and Deep Structure of the Cis-Baikal Region* (Nauka, Novosibirsk, 1978), pp. 101–107 [in Russian].
6. F. W. Klein, *Hypocenter Location Program HYPOINVERSE. Part 1. Users Guide to Versions 1, 2, 3, and 4* (U.S. Geol. Surv. Open File Report 78-694, 1978).
7. S. V. Krylov, M. M. Mandel'baum, V. S. Seleznev, et al., "Detailed Deep Seismic Studies in the Upper Angara Area of the Baikal Rift Zone," Geol. Geofiz., No. 7, 17–27 (1990).
8. K. G. Levi, A. V. Solonenko, V. M. Kochetkov, et al., "Recent Geodynamics: Seismology, Active Faults, and Seismotectonics (Basic Aspects)," in *Lithosphere of Central Asia* (Nauka, Novosibirsk, 1996), pp. 134–149 [in Russian].
9. I. V. Lobachevskii and S. I. Golenetskii, "Interpretation of Regional Gravity Anomalies and Seismicity of the Northeastern Cis-Baikal Region," Geol. Geofiz., No. 1, 101–109 (1979).
10. Ma Tzin, Ma Senli, Lyu Lichan, et al., "Experimental Study of Successive Motions on Intersecting Faults and Block Movements," in *M.V. Gzovskii and Development of Geophysics* (Nauka, Moscow, 2000), pp. 207–219 [in Russian].
11. V. D. Mats, G. F. Ufimtsev, and M. M. Mandel'baum, *The Cenozoic of the Baikal Rift Basin: Structure and*

Geological History (SO RAN GEO, Novosibirsk, 2001) [in Russian].

12. V. I. Melnikova and N. A. Radziminovich, "Focal Mechanisms of Baikal Earthquakes of 1991–1996," Geol. Geofiz. **39** (11), 1598–1607 (1998).
13. V. I. Melnikova, N. A. Gileva, R. A. Kurushin, et al., "Tentative Location of Areas for Yearly Reviews of Seismicity in the Cis- and Trans-Baikal Region," in *Earthquakes of 1997 in North Eurasia* (FOP, Obninsk, 2003), pp. 107–117 [in Russian].
14. V. I. Melnikova, N. A. Gileva, N. A. Radziminovich, et al., "The Kichera Earthquakes (Mw = 6.0 and 5.6; I_0 = 7–8) of March 21, 1999, in the Cis-Baikal Region," in *Earthquakes of 1999 in North Eurasia* (FOP, Obninsk, 2005), pp. 280–295 [in Russian].
15. *New Catalog of Strong Earthquakes in the USSR* (Nauka, Moscow, 1977) [in Russian].
16. B. M. Pis'mennyi and A. M. Alakshin, "On the Inner Structure of Rift Basins in the Northern Cis-Baikal Region," Geol. Geofiz., No. 8, 46–51 (1980).
17. N. A. Radziminovich, V. I. Melnikova, B. M. Koz'min, and N. V. Tatomir, "The Oldongsinskii Swarm of Earthquakes of 1997–2002 on the Northeastern Flank of the Baikal Rift Zone," in *Geodynamics and Environmental Geological Changes in Northern Regions: Proc. All-Russia Conf. with Participation of Foreign Specialists (Arkhangelsk, September 13–18, 2004)* (2004), pp. 193–196 [in Russian].
18. N. A. Radziminovich, V. I. Melnikova, and V. A. San'kov, "Seismotectonic Crustal Deformations at the Southern Termination of the Baikal Basin," in *Recent Geodynamics and Hazardous Natural Processes in Central Asia,* Ed. by K. G. Levi and S. I. Sherman (Inst. Zemnoi Kory SO RAN, Irkutsk, 2005), pp. 141–144 [in Russian].
19. Yu. V. Riznichenko, "Calculation of the Strain Rate during the Seismic Flow of Rock Masses," Izv. Akad. Nauk SSSR, Ser. Fiz. Zemli, No. 10, 23–31 (1977).
20. *Seismotectonics and Seismicity of the Cis-Baikal Rift System*, Ed. by V. P. Solonenko (Nauka, Moscow, 1968) [in Russian].
21. S. I. Sherman, K. Zh. Seminskii, S. A. Bornyakov, et al., *Faulting in the Lithosphere: Extension Zones* (Nauka, Novosibirsk, 1992) [in Russian].
22. N. V. Solonenko and A. V. Solonenko, *Aftershock Sequences and Earthquake Swarms in the Baikal Rift Zone* (Nauka, Novosibirsk, 1987) [in Russian].
23. A. V. Solonenko, N. V. Solonenko, V. I. Melnikova, et al., "Stresses and Motions in Earthquake Sources of Siberia and Mongolia," in *Seismicity and Seismic Regionalization of North Eurasia* (IFZ RAN, Moscow, 1993), Issue 1, pp. 113–122 [in Russian].
24. N. A. Sycheva, S. L. Yunga, L. M. Bogomolov, and V. A. Mukhamadeeva, "Determination of Seismotectonic Crustal Strains in the North Tien Shan Using Focal Mechanisms from Data of the KNET Digital Seismic Network," Fiz. Zemli, No. 11, 62–78 (2005) [Izvestiya, Phys. Solid Earth **41**, 916–930 (2005)].
25. S. L. Yunga, *Methods and Results of a Study of Seismotectonic Deformations* (Nauka, Moscow, 1990) [in Russian].
26. S. L. Yunga, "Comparative Analysis of Seismotectonic Deformations in Areas of Active Geodynamic Regimes," in *Geophysics at the Century Threshold* (OIFZ RAN, Moscow, 1999), pp. 253–264 [in Russian].
27. Yu. A. Zorin, E. Kh. Turutanov, and V. M. Kozhevnikov, "Geophysical Constraints on Mantle Plumes beneath the Baikal Rift Zone and Its Vicinities," Dokl. Akad. Nauk **393** (5), 677–680 (2003).